LIMNOLOGY
AND
OCEANOGRAPHY

September 2002
Volume 47
Number 5

Limnol. Oceanogr., 47(5), 2002, 1273–1282

The volume scattering function of natural bubble populations

Xiaodong Zhang[1] *and Marlon Lewis*
Department of Oceanography, Dalhousie University, Halifax, Nova Scotia, Canada B3H 4J1

Michael Lee
Marine Hydrophysical Institute, National Academy of Sciences of Ukraine, Sevastopol, Crimea, Ukraine 99011

Bruce Johnson
Department of Oceanography, Dalhousie University, Halifax, Nova Scotia, Canada B3H 4J1

Gennady Korotaev
Marine Hydrophysical Institute, National Academy of Sciences of Ukraine, Sevastopol, Crimea, Ukraine 99011

Abstract

The volume scattering function (VSF) of natural bubble populations is (1) determined from Mie scattering theory, (2) measured by a newly designed volume scattering meter in the laboratory, and (3) inferred from field observations of the VSF. The laboratory measurements have confirmed our theoretical prediction in that (1) bubbles of sizes that have been recorded in situ in the surface ocean (>10 μm) show elevated scattering for angles between 60° and 80° and (2) the organic coatings on the bubble surface will increase the scattering in the backward hemisphere but little change the scattering in the forward directions, including the critical angles. An optimization analysis is applied to the measurement of the VSF in coastal waters, and the results suggest the potential existence of submicron bubbles that are coated with organic film. The bubble population thus determined, which has a negligible contribution to the total scattering (5%), accounts for 40% of the total backscattering that has been observed in situ. The extension of the bubble size distribution to smaller sizes than can presently be measured by direct techniques will alter the shape of derived phase function in general but will result in rather small changes to the backscattering ratio (<20%) as long as the slope of the size distribution is small, because most of the changes are in the forward ($<10°$) direction. However, the prominent peak in the VSF at the critical angle observed for larger bubbles is strongly reduced by the inclusion of the small sizes, and the backscattering ratio is increased by a factor of two for distributions that varies as the -4 power of size. Because these bubbles contribute strongly to scattering at large angles, these results have significant implications for the remote observation of the color of the sea.

Remote observations of the spectral distribution of light backscattered from the upper ocean provide the only practical means for diagnosing the spatial and temporal variations of near-surface phytoplankton concentration in the ocean (Gordon and Morel 1983; McClain 1993). These data provide useful input into evaluations of carbon flux and primary production (e.g., Smith and Baker 1982; Morel 1991; Field et al. 1998; Behrenfeld et al. 2001), upper ocean heat flux (e.g., Lewis et al. 1990), large-scale phenomena such as the El Niño-Southern Oscillation (ENSO) variations (e.g., Feldman et al. 1984; Chavez et al. 1999), and scientific analysis and management of the coastal zone (Pernetta and Milliman 1995).

Because of their strong absorption in the blue, phytoplankton pigments are the major determinant of the spectral distribution of water-leaving radiance (''ocean color''). The amplitude of the signal, however, relates largely to the backscattering coefficient. Laboratory observations of vari-

[1] Present address: John D. Odegard School of Aerospace Sciences, University of North Dakota, Grand Forks, North Dakota 58202-9007.

Acknowledgments

This work was supported by the Office of Naval Research Hyperspectral Coastal Ocean Dynamics Experiment program, the Natural Sciences and Engineering Research Council (Canada), and Satlantic, Inc., under grants to the Science and Technology Center of the Ukraine. We thank Eugeny Shibanov for processing of the VSM data and Regina Maass for assistance in the laboratory experiments. We are also grateful to Emmanuel Boss, André Morel, and Scott Pegau for discussions, advice, and inspiration.

ous phytoplankton species confirm that their backscattering efficiency is very low (Ahn et al. 1992), a result that is consistent with theory (Morel and Bricaud 1981). Paradoxically, the concentration of phytoplankton, a major product derived from ocean color remote sensing, only accounts for 5%–10% of the particulate backscattering that sets the scale for the water-leaving radiance (Morel and Ahn 1991; Zhang et al. 1998). There continues to be uncertainty with respect to the sources of variability in the backscattering process in the upper ocean.

Zhang et al. (1998) proposed that microbubbles in the upper ocean could be responsible for a large portion of oceanic backscattering. On the basis of average in situ measurements of the bubble size distribution and number density, they calculated the total volume scattering and backscattering coefficients for typical oceanic bubble populations. They found, as well, that organic coatings on the bubble surface significantly enhance the backscattering efficiency but barely alter the total scattering. Bubbles can therefore potentially explain the amplitude of observed backscattering in the ocean and, through a general increase in the spectral water-leaving radiance, can change the relative proportion of light in the blue and green wavelengths used to compute ocean phytoplankton concentration.

Herein, we examine the angular distribution of the scattering of light by natural populations of bubbles in the ocean. The resulting volume scattering function (VSF), so derived, completely determines the optical properties of bubbles because absorption is negligible, except for very heavy coatings of organic matter with a very high imaginary index ($\sim$0.006; Zhang et al. 1998). We present herein the VSF for both single bubbles and bubble populations with various size distributions. The theoretical result is compared with new, high-precision, laboratory measurement of the VSF of artificially produced bubbles in natural seawater of known size distribution. The effects on the derived phase function by smaller bubbles, whose existence and number density are still uncertain, are analyzed. Finally, measurements of the VSF of surface waters at sea are examined during a transition from high winds to low, with a view toward the use of these novel observations to infer the nature of bubble populations introduced into the ocean by breaking waves.

Theory and background

VSF—The VSF $\beta(\psi)$ is radiometrically defined as the radiant intensity, I, derived from a volume element in a given direction (ψ), per unit of incident irradiance (E) and per unit volume (V)—i.e.,

$$\beta(\psi) = \frac{I(\psi)}{EV} \quad (\mathrm{m}^{-1}\ \mathrm{sr}^{-1}) \tag{1}$$

For a group of particles, e.g., a bubble population, the VSF $\beta(\psi)$ is computed as

$$\beta(\psi) = \int_{r_{\min}}^{r_{\max}} Q_\beta(\psi, r)\pi r^2 n(r)\, dr \tag{2}$$

where $Q_\beta(\psi, r)$, with units of sr^{-1}, is the scattering efficiency per unit solid angle in the direction ψ for a particle of size r and can be calculated by Mie theory if the particle is spherical (e.g., Bohren and Huffman 1983). The $n(r)$ ($\mathrm{m}^{-3}\ \mu\mathrm{m}^{-1}$) is the particle number-size distribution, which represents the particle number per unit volume per unit radius interval at radius r. The limits $r_{\min}$ and $r_{\max}$ denote the minimum and maximum radius of the particle population. We used Eq. 2 to calculate the VSF of a bubble population.

The total volume scattering coefficient, b (m^{-1}), is given by

$$b = 2\pi \int_{\psi=0}^{2\pi} \beta(\psi)\sin(\psi)\, d\psi \quad (\mathrm{m}^{-1}) \tag{3}$$

Note that the lower integration limit of Eq. 3 is normally not zero in practice because of instrumentational limitations, such as finite acceptance angles of the sensor (e.g., AC-9) or spurious measurement at small angles (e.g., volume scattering meter [VSM]; *see below*). Similarly, the upper limit is not 2π either. This will lead to an underestimate of the total scattering coefficient, mostly because of omissions of scattering at small angles. The VSF normalized by the total scattering (also called phase function), $\tilde{\beta}(\psi) = [\beta(\psi)]/b$ (sr^{-1}), provides information about the relative angular distribution of the scattering.

If we express the bubble size distribution $n(r)$ as

$$n(r) = N_0 p(r) \tag{4}$$

where N_0 (m^{-3}) is the total bubble number density in a unit volume of water and $p(r)$ ($\mu\mathrm{m}^{-1}$) is the bubble probability density function at radius r, then $\tilde{\beta}$ depends solely on the size distribution [$p(r)$] and not on the total bubble number density. The backscattering ratio, which describes the proportion of the light scattered in the backward hemisphere to the total scattering, can be derived as

$$\tilde{b}_b = 2\pi \int_{\psi=\pi/2}^{\pi} \tilde{\beta}(\psi)\sin(\psi)\, d\psi \tag{5}$$

Characteristics of natural bubble populations—Despite application of various techniques, including holography (O'Hern et al. 1988), optical reflection (Su et al. 1988), sound speed (Farmer and Vagle 1989), or acoustic backscatter (Vagle and Farmer 1992), the minimum bubble size for a bubble population observed to date in the ocean is $\sim$10 μm. This, however, should be interpreted as a resolution limit of the instruments. Holography could not distinguish a bubble from a particle $<$10 μm (O'Hern et al. 1988). The linearity of the calibration curve used for the optical reflection method (Su et al. 1988) is valid only for bubbles $>$10 μm (Su et al. 1994). The acoustic resonance frequency for a 10-μm bubble is $\sim$325 kHz at the surface and will increase with depth (Clay and Medwin 1977). In bubble detection, the highest frequency that has been used to date is 200 kHz, except in Vagle and Farmer's experiment (Vagle and Farmer 1992), during which one frequency of 400 kHz (bubble resonant size of 8 μm) was used. However, they also indicated

that the off-resonant contribution from larger bubbles (Commander and Moritz 1989) is very large at this frequency, making it difficult, if not impossible, to deduce the bubble density at that size.

There have been no in situ observations for smaller bubbles. Under laboratory conditions, however, stable bubbles between 1 and 10 μm have been observed in both fresh- and seawater (Gavrilov 1969; Johnson and Cooke 1981). Yount et al. (1984) estimated that cavitation nuclei of radii from 0.1 to 1 μm in distilled water exist at densities of $\sim 4 \times 10^{10}$ m^{-3}. Cavitation nuclei are the preexisting seed nuclei (gas inclusions) within a liquid from which bubbles can grow. It is expected that seawater will host more bubbles than freshwater (Cartmill and Su 1993; Haines and Johnson 1995).

Immediately after wave breaking, entrained bubbles can be >1 mm (Deane 1997, 1999). These large bubbles quickly rise to the surface, leaving behind a diffuse cloud of microbubbles (Lamarre and Melville 1991). The measured maximum bubble size for the resident bubble population with some persistence is about several hundred microns (e.g., Medwin 1977; Johnson and Cooke 1979).

Early bubble measurements that used photographic methods (Kolovayev 1976; Johnson and Cooke 1979) suggested a modal distribution with reported peak radius varying between 40 and 100 μm. This contradicted the acoustical measurements (Medwin 1970, 1977; Medwin and Breitz 1989), which showed that the bubble density continued to increase as the radius decreased from 60 to ~ 15 μm. Walsh and Mulhearn (1987) suggested that the photographic observations lack the resolution to discriminate smaller bubbles; however, Su et al. (1988), using an optical device based on dark-field specular reflection, confirmed a peak located at ~ 20 μm. Using an acoustical-backscatter technique, Farmer and Vagle (1989) measured bubbles between 8 and 130 μm with a peak at ~ 20 μm.

From these disparate results, it is difficult to define the general form of the bubble distribution in water or whether it follows a modal (e.g., Gaussian) or monotonic distribution. However, for the larger part (right side of the peak) of the modal distribution or for the entire monotonic distribution, the bubble probability density function, $p(r)$, is found to follow a power law in general—i.e.,

$$p(r) \propto r^{\xi} \tag{6}$$

Reported values for the exponent ξ have been between -3 and -7 (Johnson and Cooke 1979; Walsh and Mulhearn 1987; O'Hern et al. 1988; Su et al. 1988; Vagle and Farmer 1992; Su and Cartmill 1994; Terrill et al. 2001). The value of ξ has also been found to change for small and large portions of the bubble distribution, and the pattern of the variation is different for bubbles of different origins.

For example, for wind-generated bubbles, Garrett et al. (2000) suggested, on the basis of dimensional grounds, that the initial bubble size spectrum has $\xi = -10/3$; dissolution and rising under buoyancy will modify the spectrum such that the slope is $\xi + 1 (\approx -2)$ for bubbles <100 μm and $\xi - 2 (\approx -5)$ for bubbles >100 μm. This is consistent with the result observed by Su et al. (1988) and Terrill et al. (2001) under windy conditions. This, however, disagrees with the data from Medwin and Breitz (1989), which showed ξ being -4 for bubbles <50 μm and -2.6 for large bubbles. Wu (1994) suggested that these data, especially at large sizes, actually represented newly generated bubbles.

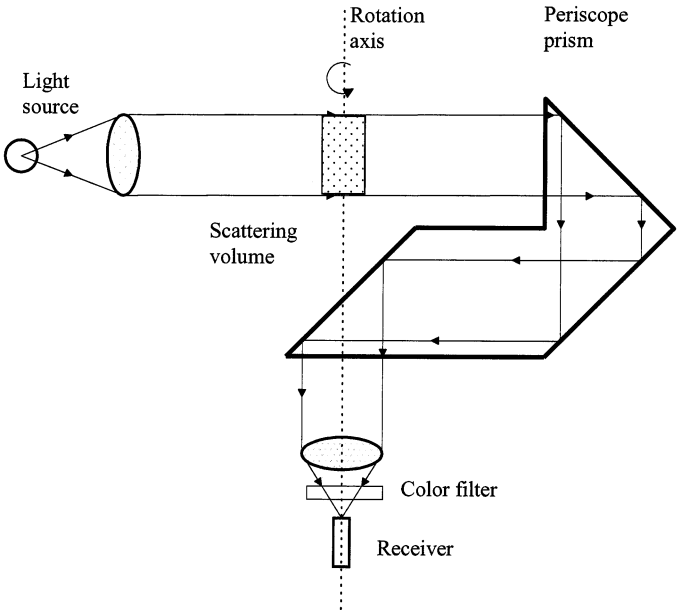

Fig. 1. Schematic diagram of the VSM. The scattering volume changes over the course of measurement, with the volume ≈ 5.76 cm^3 for 90° viewing.

It has also been suggested that the number density of bubbles from other sources would have different size dependence. Cavitation nuclei (<60 μm) observed in relatively calm seas (Medwin 1977; O'Hern et al. 1988) have a ξ of -4 (Mulhearn 1981), and bubble populations (>60 μm) formed from biological activity or outgassing by decayed sediment have a slope of -2 (Medwin 1970, 1977; Mulhearn 1981). Woolf and Thorpe (1991) found that -4 fitted most of the results reasonably well, and it was also in agreement with their model simulations.

Finally, once generated, natural bubbles with sizes <300 μm are coated with a layer of organic film on a timescale of seconds, and only for a very small part of their lifetime can bubbles be considered clean (Thorpe 1982). The organic film will help stabilize microbubbles by altering buoyancy and blocking gas transfer (Yount 1979) or by providing mechanical strength (Johnson and Wangersky 1987). The thickness of the organic coating for oceanic bubbles ranges from 0.01 μm for lipids such as fatty esters, fatty acids, and fatty alcohols to 1 μm for proteins such as glycoproteins and proteoglycans (*see* Zhang 1998).

Methodology

Mie calculation—The deformation from sphericity for a rising bubble of size 500 μm is only 4% (Thorpe 1982). Therefore, natural persistent bubbles can be assumed to be spherical for all practical purposes, and Mie theory (Bohren and Huffman 1983) can be used to calculate the angular scattering efficiency $[Q_\beta(\psi, r)]$ for clean and coated bubbles.

The refractive index of bubbles relative to water is 0.75. The maximum bubble radius is set to be 300 μm, and the minimum radius varies from 0.1 to 10 μm. The organic coating is assumed to be of protein origin (the refractive index relative to water is 1.2; Aas 1981), with a thickness of 0.1 μm. For comparison purposes, we also calculated $Q_\beta(\psi, r)$ for other particles with relative indices of 1.02, 1.05, 1.10, 1.15, and 1.20. The bubble size distributions were simulated by use of two general forms; one is a Junge distribution (Eq. 6), and the other is a normal distribution (to simulate modal distribution).

VSM—A new VSM has been designed to provide measurement of the VSF at high angular resolution (Lee and Lewis unpubl. data). A schematic diagram of the VSM is shown in Fig. 1. The salient design features of this instrument are that, unlike previous VSMs (e.g., Kullenberg 1968; Petzold 1972), the light source and receiver are fixed in position, whereas the angular measurement of scattering is achieved by rotating a newly designed periscope prism. This arrangement simplifies the scanning mechanism and allows a high angular resolution (0.3°) with a beam path length of 0.2 m, a beam divergence of 0.1°, and a receiver acceptance angle that varies from 0.2° to 1°. VSFs over the full angular range can be measured with a single run, which takes 1.5 min. The final VSF is the average of the measurements from 0° to 180° and from 360° to 180°. During the measurement, a filter centered at 555 nm is used to provide spectral conditioning of the received signal.

Because of spurious scattering contamination for small angles and angles close to 180°, the measurements made in the laboratory were reliable only from 10° to 170°, although recent improvements to the device have extended the useful angular coverage to the range from 0.6° to 178° (Lee and Lewis unpubl. data). The restricted version of the measurements permits us to only examine the relative VSF (phase function) for these measurements. Improvements to the instrument for the field deployment (*see below*) allowed the accurate determinations of the VSF, and the total scattering coefficient is obtained by integration of the VSF (Eq. 3) within the new angular range (no extrapolation is applied). The total scattering coefficient estimated this way is comparable to the measurement by an AC-9 (WetLabs, Inc.), which has an acceptance angle of 0.7° in water.

VSF measurements of controlled bubble populations—Natural seawater ($S \sim 35$) was passed through inline filters twice under normal tap water pressure, first through a 1.5-μm filter and then through a 0.2-μm filter. The seawater then flowed into a glass column (20 cm diameter and 40 cm length) and was bubbled by passing gas through three sintered glass frits (4–10 μm pore size), to strip dissolved surface-active material. The seawater was introduced at the top of the column and removed from the bottom, thus flowing counter to bubble rise. The resident time of the water in the column was ~20 min. Adsorbed organic material was collected as the bubbles collapsed at the surface and used later as a source of added surfactant. All fittings for the bubbling column were made of Pyrex or Teflon, and all surfaces were carefully cleaned before use. The air used to generate bubbles was passed through a water trap, an active charcoal column, and a 0.2-μm filter.

Bubbles for analysis were generated at a cylindrical frit surface by application of a shear field (Johnson and Gershey 1991). Bubbles produced in this way follow a normal distribution whose mean and standard deviation can be controlled by adjusting water and air flow rate and the pore size of the frit. The controllable mean radius of bubble populations ranges from 15 to 100 μm.

A well-defined bubble population with a known mean radius produced in the treated seawater was pumped into the VSM chamber continuously, while the VSF (with restricted angular range) was being determined. The measurements under these conditions are assumed to be representative of relatively clean bubbles. We then added the collected surfactant back into the prepared seawater and created the bubble population again. The measurements under these conditions are assumed to be representative of bubbles that are coated. It is recognized that it is virtually impossible to remove all surfactant materials from the water; as a consequence, bubbles in the first treatment were only relatively cleaner than those in the second.

The continuous pumping of seawater into the VSM maintained a consistent bubble number-size distribution during the measurement. Two realizations were made for each treatment (3 min) for each experiment, with each run recording the volume scattering function twice—that is, for angles between 0° and 180° and between 180° and 360°. There were no significant changes between each measurement, and the final data represent the average of the four independent realizations.

Measurements of the VSF of surface waters of the ocean—Field measurements (with improved angular range) of the VSF were carried out at the LEO-15 site off the New Jersey coast from 23 July to 04 August 2001, on board the R/V *Endeavor* in association with the Hyperspectral Coastal Ocean Dynamics Experiment. The VSM was deployed, along with an AC-9 (WetLabs, Inc.), conductivity-temperature-depth device, and other instruments, in an in-line configuration for continuous measurement during the cruise. Water was taken from the ship's intake (~5 m), and large bubbles were removed as a part of the sampling apparatus.

A dramatic change in wind speeds was experienced during this cruise, and we chose to analyze variations in the optical properties of the intake stream during this transition. The VSFs for the high- and low-wind days were used to diagnose the contributions from various particles to the observed difference. We hypothesized that the particulate contribution to the VSF could arise from (1) resuspended sediments, (2) phytoplankton, (3) detritus, and (4) bubbles (e.g., Stramski et al. 2001; Twardowski et al. 2001). Given the amplitude of the observed difference in the VSF, (β_{diff}), between high and low wind conditions, it can be partitioned into

$$\beta_{\text{diff}} = b_{\text{sus}}\bar{\beta}_{\text{sus}} + b_{\text{phy}}\bar{\beta}_{\text{phy}} + b_{\text{det}}\bar{\beta}_{\text{det}} + b_{\text{bub}}\bar{\beta}_{\text{bub}} \qquad (7)$$

where the subscripts sus, phy, det, and bub indicate the contributions from resuspended particles, phytoplankton, detritus, and bubbles, respectively. With a set of base phase functions for the four components, it is therefore possible to

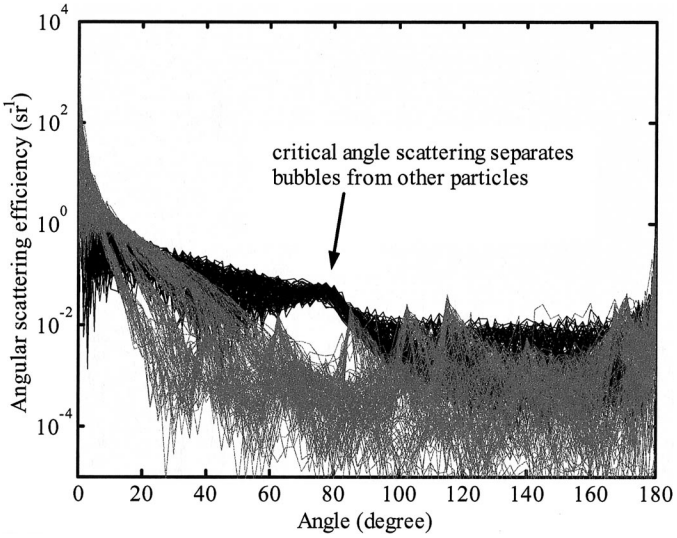

Fig. 2. The single-bubble angular scattering efficiency for bubbles (black lines) with radius between 10 and 300 μm are plotted along with the single-particle angular scattering efficiency for particles (gray lines) with refractive index of 1.02, 1.05, 1.10, 1.05, and 1.20 falling in the same size range. Note the critical angle scattering at angles between 60° and 80° separates bubbles from other particles.

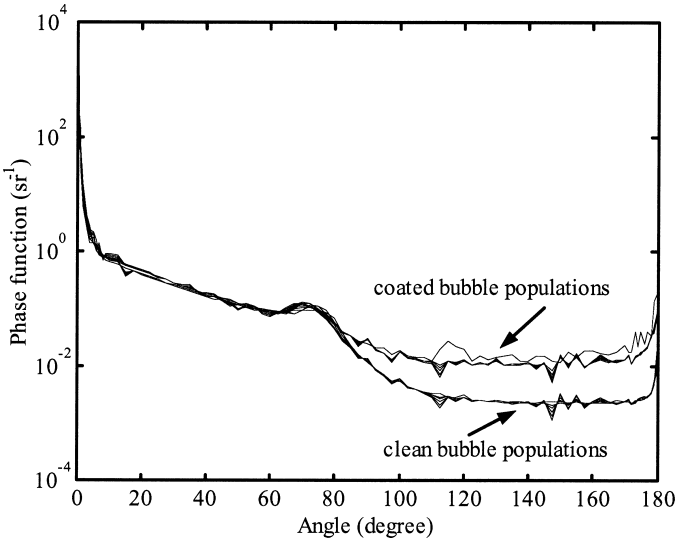

Fig. 3. The calculated phase functions for both clean and coated bubbles with different size distributions, which include populations with a Junge distribution with exponents of −3, −3.5, −4, −4.5, and −5 and a set with bubble size that followed a normal distribution, with mean radius of 25 μm and standard deviation of 10 μm. There is little effect of variations in the size distribution.

optimize Eq. 7 to find a set of the scattering coefficients that minimizes the variance between model and observation.

To achieve this, we first built the base phase functions using Mie scattering theory. The relative indices of refraction assigned to various groups of Eq. 7 were 1.15 for suspended particles, $1.05 + 0.002i$ for phytoplankton at 555 nm, 1.03 for detritus, and 0.75 for bubbles (Ahn et al. 1992; Stramski et al. 2001; Twardowski et al. 2001). We assumed that only phytoplankton absorbs light. Bubbles were also assumed to be coated with an organic film with a relative refractive index of 1.2 and a thickness of 0.05 μm. The particle size distribution, following a Junge distribution with an exponent of −4 and a minimum radius between 0.1 and 10 μm, was assumed to be the same for all the four groups. Note that even though we assumed a constant exponent of −4, varying the range in the minimum radius as we did will provide variations in the shape of the VSF that would be expected by varying the Junge exponent as well. For example, the phase function exhibited by suspended particles with a minimum radius of 0.5 μm and exponent of −5 is very similar to the phase function expected for a population with a minimum radius of 0.13 μm and an exponent of −4. For each group, therefore, we constructed 37 base VSFs. There are a total of 37^4 combinations among the four base groups within which we sought to optimize Eq. 7.

We then evaluated Eq. 7 for each combination using a global search least-squares method with the constraint that all the scattering coefficients, b_{sus}, b_{phy}, b_{det}, and b_{bub}, were nonnegative. The resultant set of scattering coefficients represented the optimal situation for this particular combination, and the one that gave the smallest residual was assumed to be closest to the reality. To assign a relatively uniform weight to all angles, the VSFs were normalized with respect to the standard deviation estimated from all the field measurements. We recognize that, given the wide range of possible variations, this solution is not wholly determinate (particularly given the uncertainties in the respective size distributions and associated phase functions) and consider our approach to be a preliminary step only rather than leading to a definitive conclusion with respect to the sources of variation in the VSF in the ocean.

Results

Mie calculations—Figure 2 shows the theoretical angular scattering efficiencies $Q_\beta(\psi, r)$ for single bubbles and for other particles (all >10 μm) with various refractive indexes. The most significant feature of the angular scattering distribution by bubbles in this size range is the elevated scattering between 60° and 80°, caused by the total reflection at the bubble surface when the incident angle is >48°. The magnitude of this critical angle scattering is at least one order of magnitude higher than the scattering by any other particles.

The effect of the bubble size distribution on the phase function of a bubble population is demonstrated in Fig. 3. We used a Junge distribution with the exponent set to −3, −3.5, −4, −4.5, and −5 and a normal distribution with mean radius of 25 μm and standard deviation of 10 μm. For a bubble population with sizes normally found in the ocean (>10 μm), the nature of the size distribution has a limited effect on the mean VSF. This is not surprising, because Zhang et al. (1998) found that the exact shape of the size distribution has virtually no impact on the mean total scattering and total backscattering coefficients of bubbles with a mean radius >4 μm. This is because the forward angular scattering efficiency does not change very much for large bubbles or particles, whereas large angle scattering is pri-

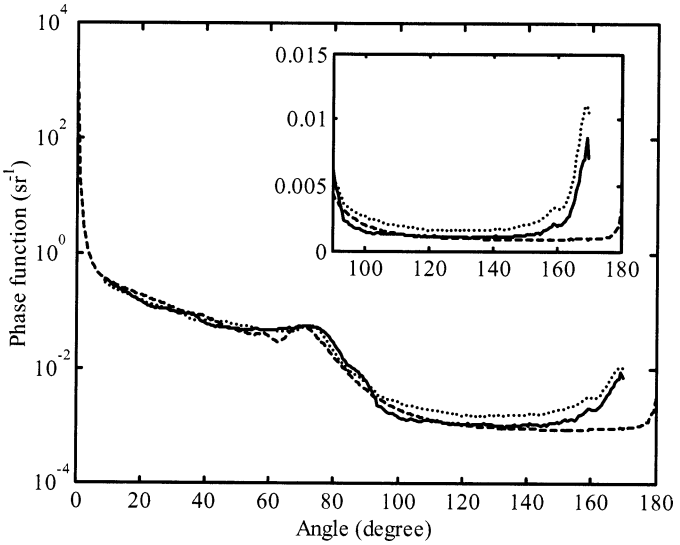

Fig. 4. Two phase functions measured for bubble populations produced in clean seawater (solid line) and in surfactant-contaminated seawater (dotted line) are compared with the theoretical phase function calculated for clean bubbles (dashed line). The bubble distribution followed a normal distribution, with a mean radius of 25 μm. Because of the reliable angular range of the measurement was from 10° and 170°, the measured data were scaled such that the integrations of the phase function between 10° and 170° for the measurements are the same as that of the theoretical calculation. The inset is in linear scale for angles from 90° to 170°.

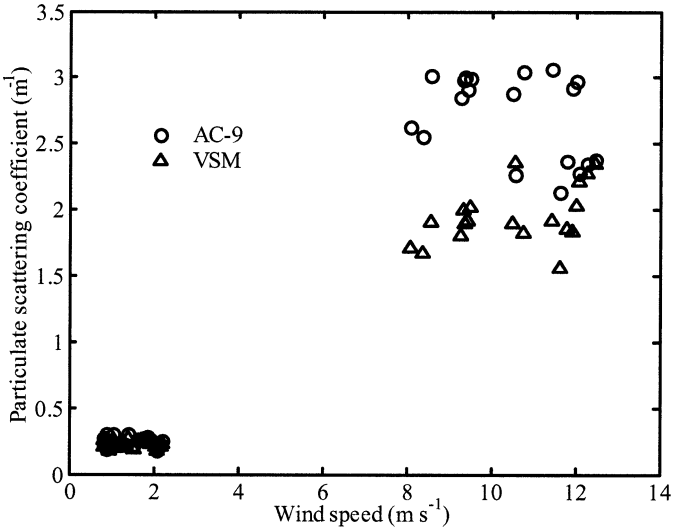

Fig. 5. The comparison of total scattering coefficient at 555 nm derived from AC-9 and the VSM for both high and low wind conditions.

marily determined by particle index and structure (Morel and Bricaud 1981; Zaneveld and Kitchen 1995). The critical angle scattering is clearly visible and is not altered with coatings (Marston et al. 1988). The coating, however, elevates the backward scattering relative to clean bubbles. The magnitude of this effect depends on the thickness and refractive index of the film. In general, coated bubbles with a protein film of 0.1 μm thickness scatter about four times more than clean bubbles between ~100° and 170°, which is consistent with our results elsewhere (Zhang et al. 1998).

It is important to note that this analysis presumes no bubbles <10 μm in size, consistent with present measurements at sea. The effect of a hypothetical distribution of bubbles with very small sizes (to 0.1 μm) can be dramatic and results in suppression of the critical angle scattering and enhanced backscattering ratios, as discussed below.

Laboratory observations of bubbles in seawater—Our theoretical results were tested with observations of a defined bubble population by use of the VSM. The bubbles produced in the laboratory experiment followed a normal distribution, but we believe that the phase function thus determined is representative of that of the natural bubble populations (>10 μm) found in the ocean, on the basis of the results presented above (*see Fig. 3*). Figure 4 shows the comparison of the phase function derived from our measurements (solid line) and the theoretical calculation (dashed line) for normally distributed clean bubbles with a mean radius of 25 μm. Because the reliable angular range of the measurement was 10°–170°, the measured data were scaled such that the integrations of the phase function between 10° and 170° for the measurement was the same as that of the theoretical calculation for the same angular range. The critical angle scattering was observed in the laboratory bubble population and its position and relative magnitude agreed well with the theoretical prediction.

The effect of the organic film coating on backscattering is also demonstrated in Fig. 4. The scattering in the backward direction was increased after surface-active materials were added and contaminated the bubbles. The backscattering ratio (estimated by use of data from 10° to 170°) increased from ~0.021 before the injection of the surfactant to ~0.032 after the injection. Zhang et al. (1998) showed that the coating on bubbles could elevate the backscattering ratio by a factor up to four, depending on the refractive index and the thickness of the organic film. The theoretically estimated backscattering ratio for clean bubbles within the same angular range was ~0.016; it is likely that our measurement of the backscattering ratio for clean bubbles was higher than the theoretical estimate because the bubbles produced in the first step were not fully devoid of organic coatings. The increased backscattering ratio should rather be interpreted such that bubbles with a thick film scatter more in the backward direction than bubbles with a thin film. As predicted, the critical angle scattering was not altered with coatings.

Although Mie theory does predict an increase of scattering by bubbles close to 180° resulting in the optical ''glory'' (Arnott and Marston 1988), our measurements showed an increase of scattering starting at 160°. We do not know the reason for this, but the increase was observed for both clean and coated bubble populations.

Derived VSFs of natural bubble populations—During the cruise off the coast of New Jersey during the summer of 2001, a continuous strong wind as high as 14 m s^{-1} (~28 knots) was recorded from 26 to 27 July, which was followed

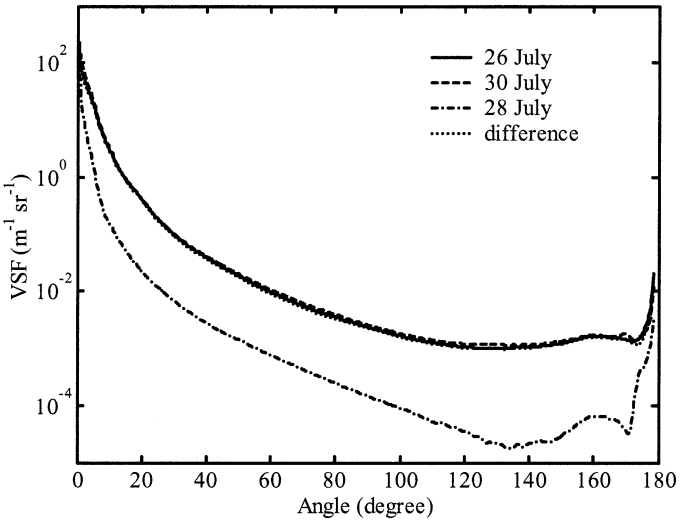

Fig. 6. The mean VSFs measured in two high-wind periods (26 and 30 July) and low wind (28 July). The line indicating the difference between the VSF for the high- and low-wind days lies on top of the VSF for the high-wind days, given the logarithmic *y* axis.

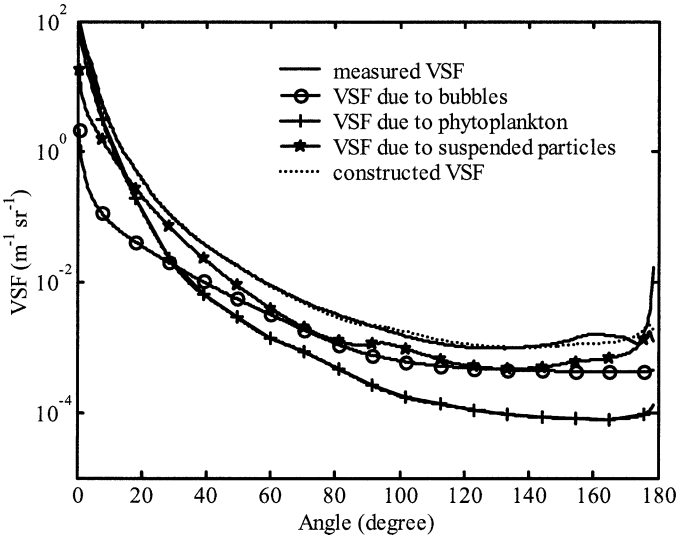

Fig. 7. The inferred VSFs with base groups of coated bubbles, phytoplankton, and resuspended particles are compared with the increased VSF measured during a transition from low to high wind. The derived scattering coefficients for bubbles, phytoplankton, and resuspended particles are 0.069, 0.86, and 0.43 m^{-1}, respectively.

by a calm period between 28 and 29 July. The wind increased again on 30 July and reached >12 m s^{-1}. In a relatively confined region (39.43°N–39.66°N, −73.34°E ∼ −73.62°E), the total scattering coefficients measured by both the AC-9 (Wetlabs, Inc.) and the VSM increased during the high-wind periods relative to the low-wind period (Fig. 5). The particulate absorption coefficient at the same wavelength also increased by ∼0.098 m^{-1} during the high-wind periods.

The measured VSFs for particulates (i.e., the VSF by pure seawater has been subtracted) are shown in Fig. 6. The VSF measurements during two high-wind periods (26 and 30 July) are almost identical in both magnitude and shape; they are however, very different from the measurements when the seas were calm (28 July). This series of measurements over short time/space scales suggests that the difference in the VSFs is due to factors resulting from changes in the local wind; these could include injection of bubbles, resuspension of mineral particles and detritus, and growth/resuspension of phytoplankton. As well, we have no way of rejecting the hypothesis that the increase is due to interaction of high sea states with the hull of the vessel as it steams or holds position. This could potentially be a source of increased bubbles as well as breaking waves.

The results of the analysis suggest that the detritus has a negligible contribution to the increased VSF because the optimizations with the least residual requires the scattering coefficient b_{det} be zero no matter which phase function from the detritus group is used. For the remaining three groups, the best fit is shown in Fig. 7, where the reconstructed VSF accounts for 94% of the variance in the measured difference spectrum. The derived VSF for resuspended particles is best represented by a population with a minimum radius of 0.15 μm, whereas a population with a minimum radius of 0.4 μm provides the best fit of the VSF for the phytoplankton group. The minimum radius for the optimal VSF for the bubble group is 0.1 μm. The total scattering coefficient derived is 1.36 m^{-1}, compared with the mean value of 1.96 m^{-1} measured by the AC-9. Contributions to the backscattering coefficient by bubbles, phytoplankton, and resuspended particles were 0.0032, 0.0008, and 0.0043 m^{-1}, respectively, which indicates the strongest contribution from bubbles and resuspended material. The derived difference in the absorption coefficient (from phytoplankton only) was 0.114 m^{-1}, which compared very well with the measured increased particulate absorption of 0.098 m^{-1} that was observed by the AC-9 at 555 nm. The derived injection of bubbles based on this best fit was 0.92×10^{12} m^{-3} for bubbles of 0.1–300 μm with a Junge exponent of −4. This will translate to a density of $\sim 10^6$ m^{-3} for bubbles of sizes >10 μm, which is the smallest size that can be measured by currently available bubble instruments. On the basis of relationships derived from literature measurements and analysis (Zhang 2001), this concentration of bubbles is what would be expected for wind speeds of ≈12 m s^{-1}, which nicely fits the conditions that existed at the time of our measurements.

Discussion and conclusions

The VSF of natural bubble populations has been investigated from three perspectives: theory, laboratory observations, and field measurements. For oceanic bubbles within the size ranges that have been measured at sea, our theoretical calculations agreed very well with the direct observations of the phase function observed for bubbles produced under controlled conditions. The prominent broad peak in the VSF at angles from 60° to 80° predicted by theory and observed in our measurements resulted from critical angle scattering at the air-water interface. This is diagnostic of bubbles whose size is larger than the wavelength of the incident light, which has been actually used in the detection

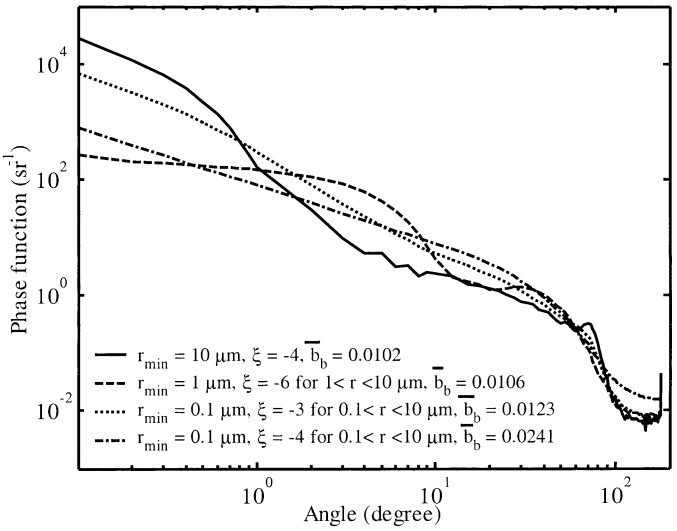

Fig. 8. The phase functions for clean bubbles with various size distributions.

of bubbles (e.g., Ling and Pao 1988). Note that as the bubble sizes approach that of the wavelength, the critical angle scattering is no longer apparent in the derived VSF.

It is impossible to directly measure the angular scattering that is due to bubble populations alone in nature. Herein, we have shown that the scattering by oceanic bubbles can be inferred from field measurements of the total VSF, even though the solution might not be unique, depending as it does directly on how well we have represented the nature of the scattering by other particles and our assumptions with regard to the size distributions of all particles.

The derived concentration of phytoplankton, however, produced absorption values that agreed with the in situ measurements, and the median size of the phytoplankton derived from the analysis was ~0.5 μm on a numerical basis. Although certain phytoplankton species could respond rapidly to an abrupt wind event, it is also conceivable that increases in detritus, mostly a decayed product of phytoplankton, would not respond as quickly.

The inversion has implied the existence of submicron bubbles with a concentration as high as 10^{12} m^{-3}. The existence of such small bubbles is questionable; they have never been observed in the ocean, although Yount et al. (1984) estimated that concentrations of cavitation nuclei of radii from 0.1 to 1 μm exist in distilled water at densities of $\sim 4 \times 10^{10}$ m^{-3} and are expected to reach higher concentrations in seawater (Cartmill and Su 1993; Haines and Johnson 1995). The concentration of larger bubbles that has been estimated from this optimization, however, is consistent with those predicted on the basis of relationships between bubble concentrations and wind speed (Zhang 2001). The bubble concentration is what would be expected for wind speeds of 12 m s^{-1}, which are similar to those observed (13 $\pm$ 2 m^{-1}).

We are unable, given the experimental protocol, to establish the degree to which these observations are representative of a wide range of conditions at sea. Given this uncertainty, it is of some interest to investigate how the shape of the VSF would be altered by differing representations of the number-size distribution of smaller bubbles. If the bubble concentration decreases rapidly at small size, then our theoretical calculations and laboratory observations of the VSF for bubbles are applicable to natural bubble populations; however, if the distribution is characterized by a continuous increase in the number density as size decreases (although clearly this must be bounded), then this could change the VSF in a way dependent on the size distribution of the small bubbles.

To address this uncertainty to some extent, we expanded the analysis presented above by allowing the Junge distribution for bubble size to extend down to 1 and 0.1 μm, using various slopes. The lower limits of radii chosen corresponded to the smallest bubbles observed under laboratory conditions for seawater (Johnson and Cooke 1981) and distilled water (Yount et al. 1984), respectively.

The original bubble size distribution we used was assumed to follow a Junge distribution with $\xi = -4$ and $r_{min} = 10$ μm, and the phase function for such a bubble population is shown in Fig. 8 as a solid line. We then extended the bubble distribution down to 1 μm following different exponents, ξ (Eq. 6), and estimated the respective phase functions on the basis of the results for clean bubbles. The general shape of the VSF, as assessed by the backscattering ratio, changes by <10% even for unrealistically steep slopes. One of the tests for $\xi = -6$ is shown in Fig. 8 as dashed lines.

Similarly, we evaluated the effect for bubbles as small as 0.1 μm. The inclusion of submicron bubbles will change the general shape of bubble phase functions considerably, depending on the concentrations of these small bubbles. For example, extending the bubble population down to 0.1 μm, following an exponent of -4, will more than double the backscattering ratio (dash-dotted lines in Fig. 8), which is the case in our inversion. However, as long as the exponent ξ of Eq. 6 is -3 (dotted lines in Fig. 8) or larger, the phase functions change by <20% in general, and, again, most of the variations are due to scattering at angles <10°. We note as well that the prominent peak in the VSF observed for critical scattering angles (60–80°) is strongly reduced with the inclusion of these small bubbles in the distribution.

The size distribution of small bubbles could be optically important in the ocean if these bubbles are present in abundance; however, the existence of significant populations of these small bubbles has not been confirmed, nor has their size distribution been measured directly. For the first time, we have provided an estimate, albeit an indirect one, of the number-size distribution of small bubbles produced under high-sea states. The reported laboratory measurement of the bubble phase function, which is determined for bubbles >10 μm, could be used for natural bubbles as long as the bubble size distributions are bounded—that is, the bubbles are >1 μm, or the number density of submicron bubbles increases with a slope of -3 or greater.

The organic coating on bubbles, which happens almost immediately after bubble genesis, will significantly change the scattering at backward angles but will exert little influence on forward scattering (Figs. 3, 4). D'Arrigo et al. (1984) characterized the bubble stabilizing substance chemically and concluded that the surfactant material is a natural

and ubiquitous degradation product of the light-harvesting chlorophyll *a*/*b* protein, which is present in almost all marine algae. Our inversion (results not shown) also suggested that the use of coated bubbles significantly improves (by >20% against the results with clean bubbles) the goodness of fit with observations. The ocean contains a large pool of such surfactant material (either dissolved or particulate), and it is more appropriate to use coated instead of clean bubbles in the simulation of the radiative transfer in the upper ocean on the basis of a full understanding of the variability in the volume scattering coefficient in the upper ocean.

It can be estimated from Fig. 7 that, for the event investigated, phytoplankton contributed to >60% of the total scattering but <10% of the total backscattering, whereas bubbles accounted for 5% of the total scattering and ~40% of the total backscattering. Our results further confirmed studies elsewhere that found that phytoplankton display very low backscattering efficiency (Morel and Ahn 1991; Stramski and Kiefer 1991) and that it is necessary to invoke other particles, such as bubbles or mineral particles (resuspended particles in this case), to explain the amplitude of light backscattered from the ocean interior (Brown and Gordon 1973; Morel and Ahn 1991; Ulloa et al. 1994; Zhang et al. 1998; Twardowski et al. 2001). Although, in coastal waters, resuspension might be important, it is envisioned that, in the open ocean, bubbles will be a dominant backscatterer, although contributions from atmospheric deposition of dust may play an important role (Twardowski et al. 2001; Claustre et al. in press). It is now recognized that the angular distribution of scattering of light in the ocean is at least as important as the integral quantity (scattering) and the absorption coefficient in determining the amplitude and spectral and angular distribution of the water-leaving radiance, which are the bases for current applications of remote sensing of ocean color (Mobley et al. 2001; Morel et al. unpubl. data). To the extent that bubble populations in the ocean contribute a significant fraction of the backscattered light and to the extent that their concentration and perhaps size distribution are variable over a range of time- and space scales, these results are of considerable significance for an accurate diagnosis of biological processes from remotely sensed observations of ocean color.

References

AAS, E. 1981. The refractive index of phytoplankton, 46. Institutt for Geofysikk, Universitetet i Oslo.

AHN, Y.-H., A. BRICAUD, AND A. MOREL. 1992. Light backscattering efficiency and related properties of some phytoplankters. Deep-Sea Res. **39:** 1835–1855.

ARNOTT, W., AND P. L. MARSTON. 1988. Optical glory of small freely rising gas bubbles in water: Observed and computed cross-polarized backscattering patterns. J. Opt. Soc. Am. **5:** 496–506.

BEHRENFELD, M. J., AND OTHERS. 2001. Biospheric primary production during an ENSO transition. Science **291:** 2594–2597.

BOHREN, C. F., AND D. R. HUFFMAN. 1983. Absorption and scattering of light by small particles. John Wiley & Sons.

BROWN, O. B., AND H. R. GORDON. 1973. Two component Mie scattering models of Sargasso Sea particles. Appl. Opt. **17:** 2461–2465.

CARTMILL, J., AND M.-Y. SU. 1993. Bubble size distribution under saltwater and freshwater breaking waves. Dyn. Atmos. Oceans **20:** 25–31.

CHAVEZ, F. P., P. G. STRUTTON, G. E. FRIEDERICH, R. A. FEELY, G. C. FELDMAN, D. G. FOLEY, AND M. J. MCPHADEN. 1999. Biological and chemical response of the equatorial Pacific Ocean to the 1997–98 El Nino. Science **286:** 2126–2131.

CLAUSTRE, H., AND OTHERS. In press. Is desert dust making oligotrophic waters greener? Geophys. Res. Lett.

CLAY, C. S., AND H. MEDWIN. 1977. Acoustical oceanography: Principles and applications. John Wiley & Sons.

COMMANDER, K. W., AND E. MORITZ. 1989. Off-resonance contributions to acoustical bubble spectra. J. Acoust. Soc. Am. **85:** 2665–2669.

D'ARRIGO, J. S., C. SAIZ-JIMENEZ, AND N. S. REIMER. 1984. Geochemical properties and biochemical composition of the surfactant mixture surrounding natural microbubbles in aqueous media. J. Colloid Interface Sci. **100:** 96–105.

DEANE, G. B. 1997. Sound generation and air entrainment by breaking waves in the surf zone. J. Acoust. Soc. Am. **192:** 2671–2689.

———. 1999. Air entrainment processes and bubble size distribution in the surf zone. J. Phys. Oceanogr. **29:** 1393–1403.

FARMER, D. M., AND S. VAGLE. 1989. Waveguide propagation of ambient sound in the ocean-surface bubble layer. J. Acoust. Soc. Am. **86:** 1897–1808.

FELDMAN, G. C., D. CLARK, AND D. HALPERN. 1984. Satellite color observations of the plankton distribution in the eastern equatorial Pacific during the 1982–1983 El Niño. Science **226:** 1069–1071.

FIELD, C. B., M. J. BEHRENFELD, J. T. RANDERSON, AND P. G. FALKOWSKI. 1998. Primary production of the biosphere: Integrating terrestrial and oceanic components. Science **281:** 237–240.

GARRETT, C., M. LI, AND D. M. FARMER. 2000. The connection between bubble size spectra and energy dissipation rates in the upper ocean. J. Phys. Oceanogr. **30:** 2163–2171.

GAVRILOV, L. R. 1969. On the size distribution of gas bubbles in water. Sov. Phys. Acoust. **15:** 22–24.

GORDON, H. R., AND A. MOREL. 1983. Remote assessment of ocean color for interpretation of satellite visible imagery, a review. Springer-Verlag.

HAINES, M. A., AND B. D. JOHNSON. 1995. Injected bubble populations in seawater and fresh water measured by a photographic method. J. Geophys. Res. **100:** 7057–7068.

JOHNSON, B. D., AND R. C. COOKE. 1979. Bubble populations and spectra in coastal waters. A photographic approach. J. Geophys. Res. **84:** 3761–3766.

———, AND ———. 1981. Generation of stabilized microbubbles in seawater. Science **213:** 209–211.

———, AND R. M. GERSHEY. 1991. Bubble formation at a cylindrical frit surface in a shear field. Chem. Eng. Sci. **46:** 2753–2756.

———, AND P. J. WANGERSKY. 1987. Microbubbles: Stabilization by monolayers of adsorbed particles. J. Geophys. Res. **92:** 14641–14647.

KOLOVAYEV, D. A. 1976. Investigation of the concentration and statistical size distribution of wind-produced bubbles in the near-surface ocean. Oceanology **15:** 659–661.

KULLENBERG, G. 1968. Scattering of light by Sargasso Sea water. Deep-Sea Res. **15:** 423–432.

LAMARRE, E., AND W. K. MELVILLE. 1991. Air entrainment and dissipation in breaking waves. Nature **351:** 469–472.

LEWIS, M. R., M.-E. CARR, G. C. FELDMAN, W. E. ESAIAS, AND C. R. MCCLAIN. 1990. Influence of penetrating solar radiation on the heat budget of the equatorial Pacific Ocean. Nature **347:** 543–545.

LING, S. C., AND H. PAO, P. 1988. Study of micro-bubbles in the

North Sea, p. 197–210. *In* B. R. Kerman [ed.], Sea surface sound. Kluwer Academic.

MARSTON, P. L., B. BILLETTE, AND C. DEAN. 1988. Scattering of light by a coated bubble in water near the critical and Brewster scattering angles. SPIE 925 Ocean Opt. IX **925:** 308–316.

MCCLAIN, C. R. 1993. Review of major CZCS applications: U.S. case studies, p. 167–188. *In* V. Barale and P. M. Schlittenhardt [eds.], Ocean colour: Theory and applications in a decade of CZCS experience. ECSC, EEC, EAEC.

MEDWIN, H. 1970. *In situ* acoustic measurements of bubble populations in coastal ocean waters. J. Geophys. Res. **75.**

———. 1977. *In situ* acoustic measurements of microbubbles at sea. J. Geophys. Res. **82:** 971–976.

———, and N. D. Breitz. 1989. Ambient and transient bubble spectral densities in quiescent seas and under spilling breakers. J. Geophys. Res. **94:** 12751–12759.

MOBLEY, C. D., L. K. SUNDMAN, AND E. BOSS. 2001. Phase function effects on oceanic light fields. Appl. Opt. **41:** 1035–1050.

MOREL, A. 1991. Light and marine photosynthesis: A spectral model with geochemical and climatological implications. Prog. Oceanogr. **26:** 263–306.

———, AND Y.-H. AHN. 1991. Optics of heterotrophic nanoflagellates and ciliates: A tentative assessment of their scattering role in oceanic waters compared to those of bacterial and algal cells. J. Mar. Res. **49:** 177–202.

———, AND A. BRICAUD. 1981. Theoretical results concerning the optics of phytoplankton, with special reference to remote sensing application, p. 313–327. *In* J. F. R. Gower [ed.], Oceanography from space. Plenum.

MULHEARN, P. J. 1981. Distribution of microbubbles in coastal waters. J. Geophys. Res. **86:** 6429–6434.

O'HERN, T. J., L. D'AGOSTINO, AND A. J. ACOSTA. 1988. Comparison of holographic and Coulter counter measurement of cavitation nuclei in the ocean. J. Fluids Eng. **110:** 200–207.

PERNETTA, J. C., AND J. D. MILLIMAN. 1995. Land-ocean interactions in the coastal zone: Implementation plan, 33. IGBP Global Change Report. IGBP.

PETZOLD, T. J. 1972. Volume scattering function for selected ocean waters. SIO Ref. 72–78. Scripps Institute of Oceanography.

SMITH, R. C., AND K. S. BAKER. 1982. Oceanic chlorophyll concentrations as determined by satellite (Nimbus-7 coastal zone color scanner). Mar. Biol. **66:** 269–279.

STRAMSKI, D., A. BRICAUD, AND A. MOREL. 2001. Modeling the inherent optical properties of the ocean based on the detailed composition of the planktonic community. Appl. Opt. **40:** 2929–2945.

———, AND D. A. KIEFER. 1991. Light scattering by microorganisms in the open ocean. Prog. Oceanogr. **28:** 343–383.

SU, M. Y., AND J. CARTMILL. 1994. Low-frequency underwater sound speed variations due to oceanic bubbles, p. 351–365. *In* M. J. Buckingham and J. R. Potter [eds.], Sea surface sound '94. World Scientific.

———, S. C. LING, AND J. CARTMILL. 1988. Optical microbubble measurements in the North Sea, p. 211–223. *In* B. R. Kerman [ed.], Sea surface sound. Kluwer Academic.

———, D. TODOROFF, AND J. CARTMILL. 1994. Laboratory comparison of acoustic and optical sensors for microbubble measurement. J. Atmos. Ocean Tech. **11:** 170–181.

TERRILL, E. J., W. K. MELVILLE, AND D. STRAMSKI. 2001. Bubble entrainment by breaking waves and their influence on optical scattering in the upper ocean. J. Geophys. Res. **106:** 16,815–16,823.

THORPE, S. A. 1982. On the clouds of bubbles formed by breaking wind waves in deep water, and their role in air-sea transfer. Phil. Trans. R. Soc. Lond. A **304:** 155–210.

TWARDOWSKI, M. S., E. BOSS, J. B. MACDONALD, W. S. PEGAU, A. H. BARNARD, AND J. R. V. ZANEVELD. 2001. A model for estimating bulk refractive index from the optical backscattering ratio and the implications for understanding particle composition in case I and case II waters. J. Geophys. Res. **106:** 14129–14142.

ULLOA, O., S. SATHYENDRANATH, AND T. PLATT. 1994. Effect of the particle-size distribution on the backscattering ratio in seawater. Appl. Opt. **33:** 7070–7077.

VAGLE, S., AND D. M. FARMER. 1992. The measurement of bubble-size distributions by acoustical backscatter. J. Atmos. Ocean Tech. **9:** 630–644.

WALSH, A. L., AND P. J. MULHEARN. 1987. Photographic measurements of bubble populations from breaking wind waves at sea. J. Geophys. Res. **92:** 14553–14565.

WOOLF, D. K., AND S. A. THORPE. 1991. Bubbles and the air-sea exchange of gases in near-saturation conditions. J. Mar. Res. **49:** 435–466.

WU, J. 1994. Bubbles in the near-surface ocean: Their various structures. J. Phys. Oceanogr. **24:** 1955–1965.

YOUNT, D. E. 1979. Skins of varying permeability. A stablization mechanism for gas cavitation nuclei. J. Acoust. Soc. Am. **65:** 1429–1439.

YOUNT, D. E., E. W. GILLARY, AND D. C. HOFFMAN. 1984. A microscopic investigation of bubble formation nuclei. J. Acoust. Soc. Am. **76:** 1511–1521.

ZANEVELD, J. R. V., AND J. C. KITCHEN. 1995. The variation in the inherent optical properties of phytoplankton near an absorption peak as determined by various models of cell structure. J. Geophys. Res. **100:** 13,309–13,320.

ZHANG, X. 1998. Light scattering by microbubbles in the ocean. Master's thesis, Dalhousie Univ.

———. 2001. Influence of bubbles on the water-leaving reflectance. Ph.D. thesis, Dalhousie Univ.

———, M. R. LEWIS, AND B. D. JOHNSON. 1998. Influence of bubbles on scattering of light in the ocean. Appl. Opt. **37:** 6525–6536.

Received: 18 June 2001
Accepted: 25 March 2002
Amended: 26 April 2002